Biofilm-induced bioclogging produces sharp interfaces in hyporheic flow, redox conditions, and microbial community structure

AGU PUBLICATIONS

Geophysical Research Letters

RESEARCH LETTER
10.1002/2017GL073651

Key Points:
- Biofilm-induced bioclogging strongly regulates hyporheic pore water flow and microbial transformation rates
- Bioclogging is primarily induced by growth of heterotrophic bacteria within pore space
- Feedbacks associated with microbial metabolism and growth generate sharp fronts in hyporheic flow, redox conditions, and microbial biomass

Correspondence to:
A. Caruso,
alice.caruso@polito.it

Citation:
Caruso, A., F. Boano, L. Ridolfi, D. L. Chopp, and A. Packman (2017), Biofilm-induced bioclogging produces sharp interfaces in hyporheic flow, redox conditions, and microbial community structure, *Geophys. Res. Lett.*, *44*, 4917–4925, doi:10.1002/2017GL073651.

Received 14 FEB 2017
Accepted 10 MAY 2017
Accepted article online 15 MAY 2017
Published online 29 MAY 2017

Biofilm-induced bioclogging produces sharp interfaces in hyporheic flow, redox conditions, and microbial community structure

Alice Caruso[1], Fulvio Boano[1], Luca Ridolfi[1], David L. Chopp[2], and Aaron Packman[3]

[1]Department of Environment, Land, and Infrastructure Engineering, Politecnico di Torino, Turin, Italy, [2]Department of Applied Mathematics, Northwestern University, Evanston, Illinois, USA, [3]Department of Civil and Environmental Engineering, Northwestern University, Evanston, Illinois, USA

Abstract Riverbed sediments host important biogeochemical processes that play a key role in nutrient dynamics. Sedimentary nutrient transformations are mediated by bacteria in the form of attached biofilms. The influence of microbial metabolic activity on the hydrochemical conditions within the hyporheic zone is poorly understood. We present a hydrobiogeochemical model to assess how the growth of heterotrophic and autotrophic biomass affects the transport and transformation of dissolved nitrogen compounds in bed form-induced hyporheic zones. Coupling between hyporheic exchange, nitrogen metabolism, and biomass growth leads to an equilibrium between permeability reduction and microbial metabolism that yields shallow hyporheic flows in a region with low permeability and high rates of microbial metabolism near the stream-sediment interface. The results show that the bioclogging caused by microbial growth can constrain rates and patterns of hyporheic fluxes and microbial transformation rate in many streams.

1. Introduction

Flow interactions between rivers and riverbeds control solute fluxes and travel times that influence hyporheic habitat, microbial metabolism, and biogeochemical transformation rates. Hyporheic and surface water chemistry both depend on sedimentary microbial processes, which are in turn influenced by influent water chemistry and pore water transport [*Grimm and Fisher*, 1984; *Findlay*, 1995; *Jones and Mulholland*, 2000; *Sophocleous*, 2002; *Boano et al.*, 2014]. These processes have been shown to regulate the export and uptake of diverse stream-borne materials of high ecological significance, including nitrogen, phosphorus, organic carbon, and metals [*Mulholland et al.*, 1997; *Harvey and Fuller*, 1998; *Fuller and Harvey*, 2000; *Mulholland et al.*, 2008; *Zarnetske et al.*, 2011; *Sawyer*, 2015]. Early models for these processes primarily relied on effective reach-scale parameterization of biogeochemical processes [*Newbold et al.*, 1981; *Bencala and Walters*, 1983; *Mulholland et al.*, 1997]. Recently, increasing process understanding and high-resolution observations has been used to develop spatially explicit models for key biogeochemical processes—most notably hyporheic nitrogen cycling—at the scale of bed forms and other river channel features that drive hyporheic flow [*Boano et al.*, 2010; *Tonina and Buffington*, 2011; *Bardini et al.*, 2012; *Zarnetske et al.*, 2012]. However, these models have not considered feedbacks between microbial growth and pore water flow. Microbial growth in streambed sediments primarily occurs in the form of biofilms that encapsulate bed sediment grains [*Battin et al.*, 2016; *Flemming et al.*, 2016]. Biofilm growth in porous media fills pore space, changes hydrologic properties of bed sediments, and diverts pore water flow in ways that regulate microbial growth and metabolism [*Suchomel et al.*, 1998; *Thullner and Baveye*, 2008; *Brovelli et al.*, 2009; *Newcomer et al.*, 2016; *Peszynska et al.*, 2016; *Coyte et al.*, 2017]. Here we present a new model that represents interactions between hyporheic exchange, microbial growth, and heterotrophic and autotrophic metabolism of nitrogen, oxygen, and organic carbon. In particular, we simulate coupling between pore water fluxes, nitrification/denitrifcation metabolism, and the reduction in permeability associated with microbial growth. While available models capture the effects of hyporheic exchange flow in stimulating microbial metabolism and biogeochemical transformation, they do not consider the consequences of the resulting biomass growth in filling pore space, reducing streambed porosity and permeability (bioclogging), and larger-scale feedbacks on rates and patterns of hyporheic exchange flow. Our model lets us assess how coupling of physical and biological processes regulates spatial distributions of microbial guilds that drive hyporheic nitrogen transformation, the associated heterogeneity

in hyporheic flow and hydrological properties (porosity and permeability), and the resulting hyporheic nitrogen transformation rates.

2. Hydraulic and Biogeochemical Model

2.1. Model Description

In this study, we provide a new model that captures the effects of multiscale coupling and feedback processes resulting from hyporheic microbial metabolism and growth. We build on prior models that represented the effects of hyporheic exchange flow, nitrogen dynamics, and heterotrophic and autotrophic metabolism, but did not account for the consequences of this metabolism in biomass growth that fills pore space and alters hyporheic flow rates and patterns. Hyporheic exchange flow, nutrient dynamics, and heterotrophic and autotrophic hyporheic nitrogen metabolism are simulated for base flow conditions in a low-gradient sand-gravel bed stream, with moderate in-stream nutrient concentrations and no carbon limitation on nitrogen metabolism.

We consider a turbulent water stream with mean water depth d and average velocity U flowing over a periodic dune-shaped riverbed composed by homogeneous and isotropic sediments. Due to the morphological periodicity, a single dune (with wavelength λ and amplitude a) and the corresponding porous media below it (depth L) are considered. As $L \gg a$ is assumed, it follows that the stream-sediment interface can be approximated as a horizontal plane in order to model the hyporheic flows in the sediments [*Elliott and Brooks*, 1997]. The domain of the mathematical problem results to be a vertical rectangle $L\text{x}\lambda$. A Cartesian reference system is adopted, where x and y represent the streamwise and upward coordinates, respectively, and the axis origin is located on the left corner of the domain bottom.

The Darcian flow induced in the sediments by the pumping process [*Elliott and Brooks*, 1997] is described by

$$\frac{\partial \theta}{\partial t} - \nabla \cdot (K \nabla h) = 0, \tag{1}$$

where $\theta(x, y, t)$ is the soil porosity, $K = K(\theta)$ is the hydraulic conductivity, and $h(x, y, t)$ is the hydraulic head distribution. We assume that dunes are not moving, and the turnover mechanism is therefore neglected. The Darcy velocity is given by $\mathbf{q}(x, y, t) = -K\nabla h$. Porosity depends on the total biomass concentration $X = (X_h + X_a)$ in the sediments

$$\theta(X) = \theta_0 - \frac{X_h}{\rho_{X_h}} - \frac{X_a}{\rho_{X_a}}, \tag{2}$$

where X_h and X_a represent the concentration (referred to the total soil volume) of heterotrophic and autotrophic biomass, respectively, and ρ_{X_h} and ρ_{X_a} are the relative densities. The subscript 0 refers to the no biomass condition. Therefore, the porosity varies in time as a function of biomass growth and decay. Hydraulic conductivity is assumed to depend on porosity according to a power law, $K = K_0(\theta/\theta_0)^j$, where the exponent is set $j = 3$. In this way, the feedback between spatiotemporal bacteria biomass dynamics, the hydraulic properties of sediments, and the hyporheic flow field is established. This formulation is used to capture the effects of microbial growth filling hyporheic pore space, and it has been found to robustly describe both physical and biological clogging processes that fill pore space by deposition and growth on grain surfaces and accumulation of deposits that bridge grain contacts. This is a multiscale formulation that captures the effects of microscale deposition, biofilm cluster growth, and pore filling on upscaled bulk permeability. Both modeling [e.g., *Clement et al.*, 1996; *Suchomel et al.*, 1998; *Thullner et al.*, 2002; *Thullner and Baveye*, 2008] and experimental [e.g., *Jaffe et al.*, 1990; *Chen et al.*, 2009, 2010] studies have adopted a power law relation, with the exponent ranging within the interval $2 \div 4$, to model clogging process caused by biofilm growth in porous media under different assumptions (e.g., heterogeneous porous media characterized by a random distribution of pore radii, different specific patterns for microbial growth, etc.). This relationship has also been applied to reproduce clogging caused by colloid filtration. Equation (2) shows that biomass growth reduces the porosity of the bed and, consequently, the permeability, influencing the solute transport within the sediments and limiting nutrient availability for microbial metabolism.

The boundary conditions for the stream water turbulent flow over the streambed, equation (1), are no flux on the lateral and lower boundary ($\partial h/\partial x|_{x=0,\lambda} = 0$ and $\partial h/\partial y|_{y=0} = 0$) and dune-induced sinusoidal head on the upper boundary, $h|_{y=L} = a_h \sin(2\pi x/\lambda - \pi/2)$, where a_h is the value of head amplitude reported by *Elliott and Brooks* [1997] based on experiments by *Vittal et al.* [1977] and *Shen et al.* [1990].

A multicomponent reactive transport model is used to predict solute fluxes and concentrations in the hyporheic zone. Four key solutes are considered: dissolved organic carbon (DOC, here considered to have the generic composition CH_2O), oxygen (O_2), ammonium (NH_4^+), and nitrate (NO_3^-). The chemical (convective and dispersive) transport and reaction in the sediments are described as

$$\theta \frac{\partial \theta c_i}{\partial t} + c_i \frac{\partial \theta}{\partial t} - \nabla \cdot (\mathbf{D_m} \nabla c_i) + \mathbf{q} \cdot \nabla c_i = R_i, \tag{3}$$

where $c_i(x, y, t)$ is the molar concentration of each compound (i = DOC, O_2, NO_3^-, and NH_4^+), $\mathbf{D_m}$ is the hydrodynamic dispersion tensor [*Bardini et al.*, 2012] and $R_i(x, y, t)$ is the consumption/production rate of i. The hydrodynamic dispersion tensor has components [*Bear and Verruijt*, 1992]

$$\theta D_{ij} = (\alpha_L - \alpha_T) \cdot \frac{q_i q_j}{|\mathbf{q}|} + \delta_{ij} \cdot \left(\alpha_T |\mathbf{q}| + \theta \cdot \tau D_{\text{mol}}\right), \tag{4}$$

where $i, j = x, y$, α_L, and α_T are the longitudinal and transversal dispersion, respectively, τ is the tortuosity, δ_{ij} is the Kroneckers delta, and D_{mol} is the molecular diffusion coefficient. Longitudinal transport is usually more pronounced than transverse transport; therefore, the values of the dispersivities α_L and α_T range in the interval $\alpha_t/\alpha_l = 1/5 \div 1/20$. Molecular diffusion is much smaller than hydrodynamic dispersion and it can be neglected.

The model includes three biochemical reactions: aerobic respiration ($CH_2O + O_2 \rightarrow CO_2 + H_2O$), denitrification ($5CH_2O + 4NO_3^- + 4H^+ \rightarrow 5CO_2 + 2N_2 + 7H_2O$), and nitrification ($NH_4^+ + 2O_2 \rightarrow NO_3^- + 2H^+ + H_2O$). The first two processes are heterotrophic and are generally induced by facultative denitrifying organisms in streambed sediments, while the third is autotrophic and is usually attributed to specific autotrophic nitrifying bacteria, such as *Nitrosomonas* and *Nitrospira* [*Mccarty*, 1971; *Hunter et al.*, 1998]. Reaction rates for organic carbon and ammonium are modeled as first order in soil porosity, chemical concentration, and heterotrophic biomass:

$$R_{\text{DOC}} = -\mu_{\text{DOC}} \theta X_h c_{\text{DOC}} \left(f_{O_2} + f_{NO_3^-}\right), \tag{5}$$

$$R_{NH_4^+} = -\mu_{NH_4^+} \theta X_a c_{NH_4^+} c_{O_2}, \tag{6}$$

where μ_{DOC} and $\mu_{NH_4^+}$ are reaction rate constants. Notice that the DOC consumption stops when oxygen and nitrate are depleted, because of the term $(f_{O_2} + f_{NO_3^-})$, while the rate of reaction of nitrification depends on the concentration of both ammonium and oxygen. In the previous reaction rates, f_{O_2} and $f_{NO_3^-}$ are equal to [*Hunter et al.*, 1998; *Bardini et al.*, 2012]

$$f_{O_2} = \begin{cases} \frac{c_{O_2}}{c_{O_2,\text{lim}}} & \text{if } c_{O_2} < c_{O_2,\text{lim}} \\ 1 & \text{if } c_{O_2} \geq c_{O_2,\text{lim}} \end{cases} \tag{7}$$

and

$$f_{NO_3^-} = (1 - f_{O_2}) \cdot \begin{cases} \frac{c_{NO_3^-}}{c_{NO_3^-,\text{lim}}} & \text{if } c_{NO_3^-} < c_{NO_3^-,\text{lim}} \\ 1 & \text{if } c_{NO_3^-} \geq c_{NO_3^-,\text{lim}}, \end{cases} \tag{8}$$

where $c_{O_2,\text{lim}}$ and $c_{NO_3^-,\text{lim}}$ are the molar limiting concentrations for oxygen and nitrate. These concentrations define conditions under which aerobic respiration and denitrification rates become linearly proportional to c_{O_2} and $c_{NO_3^-}$, respectively. Denitrification occurs only when the oxygen concentration is lower than the limiting value $c_{O_2,\text{lim}}$. Similar to other reactive transport models [*Marzadri et al.*, 2011; *Bardini et al.*, 2013], the influence of pH variation on reaction kinetics was considered to be negligible and thus omitted from the model, due to the buffering in the hyporheic zone.

Since oxygen is involved both in nitrification and aerobic respiration, its reaction rate is modeled as

$$R_{O_2} = f_{O_2} R_{\text{DOC}} + 2R_{NH_4^+}. \tag{9}$$

Finally, nitrate is a byproduct of nitrification but it is also consumed by heterotrophic bacteria by denitrification. This yields the net nitrate transformation rate

$$R_{NO_3^-} = \beta f_{NO_3^-} R_{\text{DOC}} - R_{NH_4^+}, \tag{10}$$

where $\beta = 0.8$ is a stoichiometric coefficient.

Similar to hydraulic head boundary conditions, no chemical flux conditions are set on the lower and lateral domain boundaries. At the upper boundary (i.e., the stream-sediment interface), concentrations are assumed equal to those in the stream at all times, i.e., $c_i|_{y=L} = c_{i,s}$, where subscript s refers to the stream. The same values are also set as chemical initial conditions throughout the hyporheic zone.

Bacteria are modeled using a growth-death model based on the metabolic processes described in equations (5)–(10), i.e., facultative denitrifying bacteria consume DOC by aerobic respiration and denitrification, while autotrophic bacteria consume ammonia and produce nitrate by nitrification. Net microbial growth is therefore simulated as

$$\frac{\partial X_h}{\partial t} = Y_{\mathrm{DOC}}|R_{\mathrm{DOC}}| - k_h X_h, \tag{11}$$

$$\frac{\partial X_a}{\partial t} = Y_{\mathrm{NH_4^+}}|R_{\mathrm{NH_4^+}}| - k_a X_a, \tag{12}$$

where Y_{DOC} and $Y_{\mathrm{NH_4^+}}$ are growth yields and k_h and k_a are biomass die-off rates. This is a standard formulation for biomass growth in pore spaces that have been shown to adequately represent biomass in complex system geometries, such as reactor [*Rittmann and McCarty*, 2012; *Qin and Hassanizadeh*, 2015; *Peszynska et al.*, 2016]. Initial conditions are spatially homogeneous, with $X_{h,0} > X_{a,0}$ (subscript 0 denotes $t = 0$) because autotrophic bacteria grow more slowly and are less numerous than the heterotrophic ones [*Oga et al.*, 1991; *Liu et al.*, 2004; *Ebeling et al.*, 2006]. Nonhomogeneous initial conditions of each organism are also tested to investigate the sensitivity of bioclogging process to initial biomass distributions.

2.2. Simulation Conditions

Using the approach described in the previous section, numerical simulations are carried out to investigate how the microbial growth controls the distributions of permeability, exchange flow, and nutrients. For this purpose, we employ a numerical code in COMSOL Multiphysics®, a finite element solver that uses a finite-volume approach [*COMSOL*, 2008]. A nonuniform mesh is adopted, with a higher node density near the bed surface, where the spatial gradients are higher. Specifically, 100 structured layers of quadrilateral elements are generated along the top boundary of the domain, while a free meshing technique generating an unstructured mesh is used to create triangular elements of size ranging from 0.01 m to $2.0 \cdot 10^{-5}$ m in the remaining part of the domain, for a total number of 35,064 elements.

We simulate low flow conditions in a stream with coarse sediments and no DOC limitation on nitrogen metabolism. A flow with velocity $U = 0.7$ m/s and depth $d = 0.16$ m is considered. The streambed has a hydraulic conductivity $K_0 = 10^{-3}$ m/s (characteristic of well-sorted coarse sands to gravels) and a porosity $\theta_0 = 0.3$ and is covered by bed forms with wavelength $\lambda = 1$ m and height $a = 0.1$ m [*Julien and Klaassen*, 1995]. The depth of the domain is $L = 1$ m, hence, the ratio between a and L allows us to approximate the domain as a flat bed on which a sinusoidal head variation with amplitude $a_h = 170$ Pa is imposed. We assume $\alpha_t/\alpha_l = 1/10$ [e.g., *Bardini et al.*, 2012] and choose longitudinal dispersivity of order of sediment diameter, $\alpha_l = 2 \cdot 10^{-3}$ m [*Bear*, 1988]. Solute in-stream concentrations are $c_{\mathrm{DOC};s} = 40$ mg/L, $c_{\mathrm{O_2};s} = 10$ mg/L, $c_{\mathrm{NO_3^-};s} = 1$ mg/L, and $c_{\mathrm{NH_4^+};s} = 0.05$ mg/L, while oxygen and nitrate limiting concentrations ($c_{\mathrm{O_2;lim}}$ and $c_{\mathrm{NO_3^-;lim}}$) are set at 2 mg/L and 0.2 mg/L, respectively. The initial values of biomass are imposed at $X_{h,0} = 5 \cdot 10^{-3}$ kg/m^3 and $X_{a,0} = 5 \cdot 10^{-6}$ kg/m^3. Finally, parameters describing microbial growth and metabolism have been chosen based on values reported by previous studies of heterotrophic and autotrophic biofilm growth [*Rittmann and McCarty*, 1980; *Rittmann*, 1982; *Wanner and Gujer*, 1986; *Merkey et al.*, 2009]: $\mu_{\mathrm{DOC}} = 10^{-3}$ m^3/(mg$_{X_h} \cdot d$), $\mu_{\mathrm{NH_4^+}} = 10^{-4}$ m^6/(mg$_{X_a} \cdot$ mg$_{\mathrm{O_2}} \cdot d$), $k_{d_h} = 1$ 1/d, $k_{d_a} = 1$ 1/d, $Y_{\mathrm{DOC}} = 0.16$ mg$_{\mathrm{DOC}}$/mg$_{X_h}$, $Y_{\mathrm{NH_4^+}} = 0.16$ mg$_{\mathrm{NH_4^+}}$/mg$_{X_a}$, $\rho_{X_h} = 1$ kg/m^3 and $\rho_{X_a} = 1$ kg/m^3.

In order to test the influence of initial conditions, we have also simulated a system with heterogeneous initial distribution of each microbial guild. Specifically, we have evaluated the spatial patterns of biomass and permeability starting from initial random conditions. These random functions have been extracted from two normal distribution with mean values $m_h = X_{h,0} = 5 \cdot 10^{-3}$ kg/m^3 and $m_a = X_{a,0} = 5 \cdot 10^{-6}$ kg/m^3 and standard deviations $s_h = X_{h,0} = 0.5 \cdot 10^{-3}$ kg/m^3 and $s_a = X_{a,0} = 0.5 \cdot 10^{-6}$ kg/m^3 and two uniform distributions with same mean values and width equal to $m_{h,a} \pm 3s_{h,a}$.

3. Results and Discussion

The temporal evolution of spatial patterns in permeability, pore water flow and biomass is shown in Figure 1. Sediment permeability is progressively reduced at streambed surface owing to microbial growth induced by the nitrogen, carbon, and oxygen in the exchange flow. The hydraulic conductivity progressively decreases over time (Figure 1, first row), eventually reaching a steady equilibrium configuration. The pattern of hyporheic exchange flow also changes substantially over time (Figure 1, second row) due to the clogging induced by bacterial growth, which blocks flow at depth and confines it to the near-surface zone. The results show how coupling between biofilm-induced clogging, hyporheic flow, and microbial metabolism leads to an equilibrium between permeability reduction and biomass growth characterized by sharp fronts. The homogeneous stream sediments display a strong heterogeneity at steady state, with significant hyporheic flow confined only in the shallow portion of the domain where high rates of bacterial growth occur. Therefore, the dynamics of sediment porosity, biomass concentration, and hydrodynamic flow are highly related, and the bioclogging process strongly limits the extent of hyporheic exchange. Moreover, the steady state fronts in biomass and permeability result specifically from the coupling between hyporheic fluxes, nutrient reactions, and microbial growth regardless of the initial biomass distributions. In fact, both heterotrophic and autotrophic microorganisms stratify according to the same pattern even when spatial heterogeneous initial distributions are set. Thus, the spatial heterogeneity in the microbial community does not significantly alter the hyporheic metabolism, the bulk reactions rates, and the patterns of exchange flow.

The pattern of hydraulic conductivity is very similar to the one of heterotrophic biomass, indicating that permeability is governed by the distribution of heterotrophic denitrifying organisms. The strong stratification of heterotrophic bacteria with depth in time can be observed in Figure 1 (third row). Owing to faster grow rate, heterotrophic bacteria outcompete autotrophic nitrifiers (Figure 1, fourth row) for oxygen and space, confining autotrophs to a thin layer near the sediment-water interface. In this layer, strong spatial gradients of ammonium and oxygen concentration are observed. Thus, total microbial biomass and bioclogging are both dominated by heterotrophic bacteria, and the permeability of the sediments is primarily dependent on concentration of heterotrophic biomass within the pore space. The coexistence between nitrifying and denitrifing bacteria is analyzed in *Rittmann and Manem* [1992], showing that the nitrifiers are forced deeper in the biofilm. However, the clogging mechanism is not included in the system, and this could explain the different behaviors. At steady state (Figure 1, third column), two distinct regions can be identified within the sediments: a shallower zone, characterized by advective flux, rapid solute transport, and high rates of microbial metabolism, and a deeper region that is characterized by very slow flow, nutritional depletion, and little microbial growth. This shows that both penetration of nutrients and microbial metabolism in the sediments are eventually limited by bioclogging, which induces a very strong heterogeneity within the domain, restricting hyporheic exchange, nutrient transformation, and microbial metabolism to a thin region near the sediment-water interface.

For each time reported in Figure 1, we evaluate the total hyporheic exchange flux by integrating the vertical component of Darcy velocity along the stream-bed interface ($y = 1$ m). Moreover, we calculate the total biomass and the total rates of consumption of DOC, oxygen, nitrate, and ammonium by an integration over the whole domain. The results are presented in Table 1. Hyporheic flow decreases over time as a result of an increase of microbial biomass and consequent filling of pore space in the sediments. The heterotrophic and autotrophic biomass initially grow and then decrease. The microorganisms begin to die when the stratification effect is pronounced and the nutrient inflow coming from the river does not reach the deeper area of the streambed. The reaction rates show a similar behavior of the biomass, with an initial increase followed by a reduction.

Figure 2 represents the spatial patterns in DOC, O_2, NO_3^-, NH_4^+, and microbial biomass under steady conditions. The spatial distributions of solutes and biomass concentrations show clear stratification. Distributions of key microbial functional guilds are controlled by the extent of penetration of electron acceptors from the stream. Specifically, the spatial extent of heterotrophic and autotrophic biomass is controlled by the penetration of nitrate and oxygen, respectively. The electron donors (DOC and NH_4^+) are not fully depleted, indicating that metabolism is limited by delivery of electron acceptors (nitrate and oxygen) from the water column. Strong coupling between heterotrophic metabolism, microbial growth, and permeability causes a very sharp front at the maximal extent of nitrate penetration, which can be seen to co-occur in the patterns of heterotrophic biomass (Figure 2d), nitrate (Figure 2c), permeability (Figure 1, first row), and pore water velocity

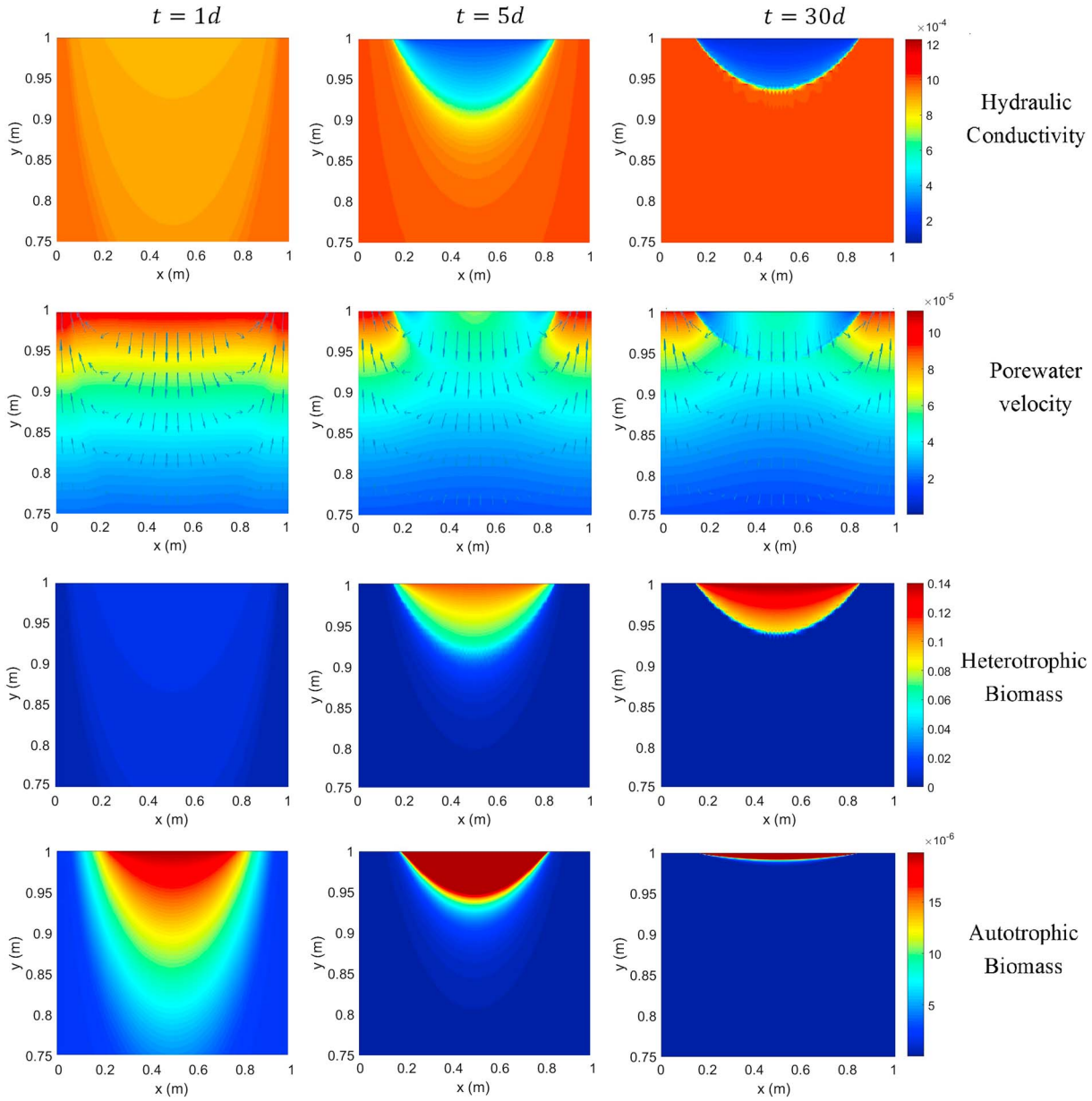

Figure 1. Temporal evolution of spatial patterns in (first row) permeability, (second row) pore water flow, and (third row) heterotrophic and (fourth row) autotrophic biomass at initial time (first column, $t = 0$ day), in the transient (second column, $t = 5$ days), and at the steady state (third column, $t = 30$ days). Warmer colors indicate higher values of the variables. The arrows in Figure 1 (second row) indicate the flow direction. Notice that the y axes have been exaggerated to evidence the patterns.

Table 1. Values of Pore Water Flow, Biomass Concentrations Per Unit Stream Width, and Reaction Rates at Different Times

	$t = 0$ day	$t = 5$ days	$t = 30$ days
q (m^2/s)	$3.16 \cdot 10^{-5}$	$2.41 \cdot 10^{-5}$	$2.24 \cdot 10^{-5}$
X_e (kg/m)	0.00410	0.00415	0.00341
X_a (kg/m)	$3.38 \cdot 10^{-6}$	$4.12 \cdot 10^{-6}$	$3.32 \cdot 10^{-5}$
R_{DOC} (kg/(m s^{-1}))	$2.61 \cdot 10^{-7}$	$2.91 \cdot 10^{-7}$	$2.47 \cdot 10^{-7}$
R_{O_2} (kg/(m s^{-1}))	$2.27 \cdot 10^{-7}$	$2.42 \cdot 10^{-7}$	$2.25 \cdot 10^{-7}$
$R_{NO_3^-}$ (kg/(m s^{-1}))	$1.41 \cdot 10^{-8}$	$2.36 \cdot 10^{-8}$	$1.80 \cdot 10^{-8}$
$R_{NH_4^+}$ (kg/(m s^{-1}))	$1.79 \cdot 10^{-10}$	$3.18 \cdot 10^{-10}$	$2.41 \cdot 10^{-9}$

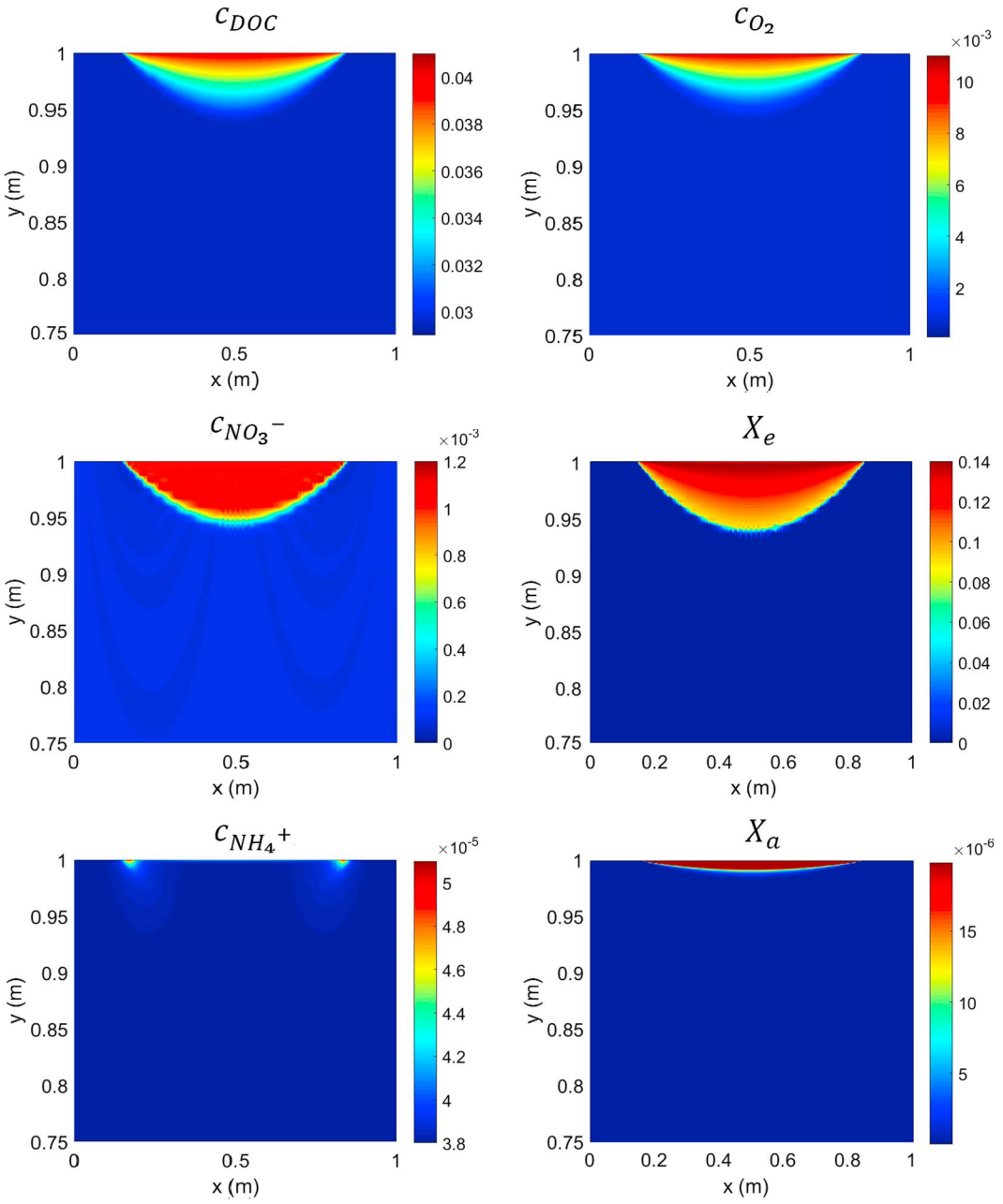

Figure 2. Expanded view of the spatial distributions of microbial biomass and chemical constituents near the sediment-water interface at steady state: (a) DOC, (b) O_2, (c) NO_3^-, (d) heterotrophic biomass, (e) NH_4^+, and (f) autotrophic biomass.

(Figure 1, second row). The sharp interface for heterotrophic growth co-occurs with the penetration of nitrate and not oxygen because these organisms are facultative, and oxygen is preferentially depleted before nitrate near the sediment-water interface. Therefore, the spatial distribution of the concentrations of DOC, O_2, and NO_3^- is most strongly influenced by heterotrophs, which occlude the pores and prevent the infiltration of nutrients to deeper sediments. Conversely, the ammonium concentration is essentially controlled by autotrophic biomass, which survives only in a very thin layer near the streambed surface where the oxygen concentration is sufficient for the growth of both species. The ammonia concentration is very low in the deeper part of the domain, owing to the low pore water fluxes into this part of the domain and the rapid metabolism of ammonia in the region of high autotrophic nitrification just under the sediment-water interface.

These results suggest that an equilibrium between nutrient exchange and microbial metabolism arises from feedback among biomass growth, reduction of permeability, and reduction of nutrient fluxes. When equilibrium is reached, two distinct zones are found: first, a superficial zone with lower hydraulic conductivity since the nutrient availability is sufficient to allow the survival of a high amount of biomass that occupies most of the porous space; second, a deeper zone with higher hydraulic conductivity, where the nutrient flux is low due to consumption by microrganisms in the surficial zone, and the biomass is not able to survive. Between these two areas, a transitional zone is present, where hydraulic conductivity, biomass, and nutrient concentrations vary sharply. The reduction of the hydraulic conductivity in the shallower zone prevents the supply of nutrients and substrates to the deeper zone, causing the biomass to die off and eventually restoring the hydraulic conductivity of the open granular sediment bed.

Microbial growth and filling of hyporheic pore spaces is expected to be a generally important control on hyporheic flow and metabolism. Our findings show that biofilm-induced bioclogging strongly regulates physical and biogeochemical processes in the hyporheic zone since it limits both exchange flux and biogeochemical transformation rates and controls the distribution of different types of microorganisms in many streams and rivers. Therefore, the coupling between hyporheic flow exchange, microbial growth, and nutrient transport is an important process that has to be better understood in order to correctly evaluate nutrient transformation rates in the hyporheic zone and the role of streambeds in nutrient cycling. Rivers are subject to additional, larger-scale complexities that will modulate the processes demonstrated here. In particular, hyporheic bioclogging should be compared with siltation-induced clogging and the frequency of sediment remobilization and invertebrate grazing, both of which disrupt biofilms, in order to evaluate in more detail the dynamics of hyporheic permeability, flow, and biogeochemistry in rivers.

References

Bardini, L., F. Boano, M. Cardenas, R. Revelli, and L. Ridolfi (2012), Nutrient cycling in bedform induced hyporheic zones, *Geochim. Cosmochim. Acta*, *84*, 47–61, doi:10.1016/j.gca.2012.01.025.

Bardini, L., F. Boano, M. Cardenas, A. Sawyer, R. Revelli, and L. Ridolfi (2013), Small-scale permeability heterogeneity has negligible effects on nutrient cycling in streambeds, *Geophys. Res. Lett.*, *40*, 1118–1122, doi:10.1002/grl.50224.

Battin, T. J., K. Besemer, M. M. Bengtsson, A. M. Romani, and A. I. Packmann (2016), The ecology and biogeochemistry of stream biofilms, *Nat. Rev. Microbiol.*, *14*(4), 251–263.

Bear, J. (1988), *Dynamics of Fluids in Porous Media*, Dover, New York.

Bear, J., and A. Verruijt (1992), *Modeling Groundwater Flow and Pollution*, D. Reidel, Dordrecht, Holland.

Bencala, K. E., and R. A. Walters (1983), Simulation of solute transport in a mountain pool-and-riffle stream: A transient storage model, *Water Resour. Res.*, *19*(3), 718–724.

Boano, F., A. Demaria, R. Revelli, and L. Ridolfi (2010), Biogeochemical zonation due to intrameander hyporheic flow, *Water Resour. Res.*, *46*, W02511, doi:10.1029/2008WR007583.

Boano, F., J. W. Harvey, A. Marion, A. I. Packman, R. Revelli, L. Ridolfi, and A. Wörman (2014), Hyporheic flow and transport processes: Mechanisms, models, and biogeochemical implications, *Rev. Geophys.*, *52*, 603–679, doi:10.1002/2012RG000417.

Brovelli, A., F. Malaguerra, and D. Barry (2009), Bioclogging in porous media: Model development and sensitivity to initial conditions, *Environ. Modell. Softw.*, *24*(5), 611–626.

Chen, C., B. L. Lau, J.-F. Gaillard, and A. I. Packman (2009), Temporal evolution of pore geometry, fluid flow, and solute transport resulting from colloid deposition, *Water Resour. Res.*, *45*, W06416, doi:10.1029/2008WR007252.

Chen, C., A. I. Packman, D. Zhang, and J.-F. Gaillard (2010), A multi-scale investigation of interfacial transport, pore fluid flow, and fine particle deposition in a sediment bed, *Water Resour. Res.*, *46*, W11560, doi:10.1029/2009WR009018.

Clement, T., B. Hooker, and R. Skeen (1996), Macroscopic models for predicting changes in saturated porous media properties caused by microbial growth, *Ground Water*, *34*(5), 934–942.

COMSOL, A. (2008), *Comsol Multiphysics Users Guide, Version 4.2*, COMSOL AB, Burlington, Mass.

Coyte, K. Z., H. Tabuteau, E. A. Gaffney, K. R. Foster, and W. M. Durham (2017), Microbial competition in porous environments can select against rapid biofilm growth, *Proc. Natl. Acad. Sci. U.S.A.*, *114*(2), E161–E170, doi:10.1073/pnas.1525228113.

Ebeling, J. M., M. B. Timmons, and J. Bisogni (2006), Engineering analysis of the stoichiometry of photoautotrophic, autotrophic, and heterotrophic removal of ammonia-nitrogen in aquaculture systems, *Aquaculture*, *257*(1), 346–358.

Elliott, A. H., and N. H. Brooks (1997), Transfer of nonsorbing solutes to a streambed with bed forms: Theory, *Water Resour. Res.*, *33*(1), 123–136, doi:10.1029/96WR02784.

Findlay, S. (1995), Importance of surface-subsurface exchange in stream ecosystems: The hyporheic zone, *Limnol. Oceanogr.*, *40*(1), 159–164.

Flemming, H.-C., J. Wingender, U. Szewzyk, P. Steinberg, S. A. Rice, and S. Kjelleberg (2016), Biofilms: An emergent form of bacterial life, *Nat. Rev. Microbiol.*, *14*(9), 563–575.

Fuller, C. C., and J. W. Harvey (2000), Reactive uptake of trace metals in the hyporheic zone of a mining-contaminated stream, Pinal Creek, Arizona, *Environ. Sci. Technol.*, *34*(7), 1150–1155.

Grimm, N. B., and S. G. Fisher (1984), Exchange between interstitial and surface water: Implications for stream metabolism and nutrient cycling, *Hydrobiologia*, *111*(3), 219–228.

Harvey, J. W., and C. C. Fuller (1998), Effect of enhanced manganese oxidation in the hyporheic zone on basin-scale geochemical mass balance, *Water Resour. Res.*, *34*(4), 623–636.

Hunter, K. S., Y. Wang, and P. Van Cappellen (1998), Kinetic modeling of microbially-driven redox chemistry of subsurface environments: Coupling transport, microbial metabolism and geochemistry, *J. Hydrol.*, *209*(1), 53–80, doi:10.1016/S0022-1694(98)00157-7.

Jaffe, P., P. Milly, and S. Taylor (1990), Biofilm growth and the related changes in the physical properties of a porous medium: 2. Permeability, *Water Resour. Res.*, *26*, 2161–2169.
Jones, J. B., and P. J. Mulholland (2000), *Streams and Ground Waters*, Academic Press, New York.
Julien, P. Y., and G. J. Klaassen (1995), Sand-dune geometry of large rivers during floods, *J. Hydraul. Eng.*, *121*(9), 657–663.
Liu, Y., S.-F. Yang, and J.-H. Tay (2004), Improved stability of aerobic granules by selecting slow-growing nitrifying bacteria, *J. Biotechnol.*, *108*(2), 161–169.
Marzadri, A., D. Tonina, and A. Bellin (2011), A semianalytical three-dimensional process-based model for hyporheic nitrogen dynamics in gravel bed rivers, *Water Resour. Res.*, *47*, W11518, doi:10.1029/2011WR010583.
Mccarty, P. L. (1971), *Energetics and Kinetics of Anaerobic Treatment*, ACS Publ., Washington, D. C.
Merkey, B. V., B. E. Rittmann, and D. L. Chopp (2009), Modeling how soluble microbial products (smp) support heterotrophic bacteria in autotroph-based biofilms, *J. Theor. Biol.*, *259*(4), 670–683.
Mulholland, P. J., E. R. Marzolf, J. R. Webster, D. R. Hart, and S. P. Hendricks (1997), Evidence that hyporheic zones increase heterotrophic metabolism and phosphorus uptake in forest streams, *Limnol. Oceanogr.*, *42*(3), 443–451.
Mulholland, P. J., et al. (2008), Stream denitrification across biomes and its response to anthropogenic nitrate loading, *Nature*, *452*(7184), 202–205.
Newbold, J. D., J. W. Elwood, R. V. O'Neill, and W. V. Winkle (1981), Measuring nutrient spiralling in streams, *Can. J. Fish. Aquat. Sci.*, *38*(7), 860–863.
Newcomer, M. E., S. S. Hubbard, J. H. Fleckenstein, U. Maier, C. Schmidt, M. Thullner, C. Ulrich, N. Flipo, and Y. Rubin (2016), Simulating bioclogging effects on dynamic riverbed permeability and infiltration, *Water Resour. Res.*, *52*, 2883–2900, doi:10.1002/2015WR018351.
Oga, T., S. Suthersan, and J. Ganczarczyk (1991), Some properties of aerobic biofilms, *Environ. Technol.*, *12*(5), 431–440.
Peszynska, M., A. Trykozko, G. Iltis, S. Schlueter, and D. Wildenschild (2016), Biofilm growth in porous media: Experiments, computational modeling at the porescale, and upscaling, *Adv. Water Resour.*, *95*, 288–301.
Qin, C.-Z., and S. M. Hassanizadeh (2015), Pore-network modeling of solute transport and biofilm growth in porous media, *Transp. Porous Media*, *110*(3), 345–367.
Rittmann, B. (1982), Comparative performance of biofilm reactor types, *Biotechnol. Bioeng.*, *24*(6), 1341–1370.
Rittmann, B., and P. McCarty (2012), *Environmental Biotechnology: Principles and Applications, McGraw-Hill Ser. in Water Resour. and Environ. Eng.*, Tata McGraw Hill Educ. Priv. Ltd., New Delhi.
Rittmann, B. E., and J. A. Manem (1992), Development and experimental evaluation of a steady-state, multispecies biofilm model, *Biotechnol. Bioeng.*, *39*(9), 914–922.
Rittmann, B. E., and P. L. McCarty (1980), Model of steady-state-biofilm kinetics, *Biotechnol. Bioeng.*, *22*(11), 2343–2357.
Sawyer, A. (2015), Enhanced removal of groundwater-borne nitrate in heterogeneous aquatic sediments, *Geophys. Res. Lett.*, *42*, 403–410, doi:10.1002/2014GL062234.
Shen, H. W., H. M. Fehlman, and C. Mendoza (1990), Bed form resistances in open channel flows, *J. Hydraul. Eng.*, *116*(6), 799–815.
Sophocleous, M. (2002), Interactions between groundwater and surface water: The state of the science, *Hydrogeol. J.*, *10*(1), 52–67, doi:10.1007/s10040-001-0170-8.
Suchomel, B. J., B. M. Chen, and M. B. Allen (1998), Macroscale properties of porous media from a network model of biofilm processes, *Transp. Porous Media*, *31*(1), 39–66.
Thullner, M., and P. Baveye (2008), Computational pore network modeling of the influence of biofilm permeability on bioclogging in porous media, *Biotechnol. Bioeng.*, *99*(6), 1337–1351.
Thullner, M., J. Zeyer, and W. Kinzelbach (2002), Influence of microbial growth on hydraulic properties of pore networks, *Transp. Porous Media*, *49*(1), 99–122.
Tonina, D., and J. M. Buffington (2011), Effects of stream discharge, alluvial depth and bar amplitude on hyporheic flow in pool-riffle channels, *Water Resour. Res.*, *47*, W08508, doi:10.1029/2010WR009140.
Vittal, N., K. Ranga Raju, and R. Garde (1977), Resistance of two dimensional triangular roughness, *J. Hydraul. Res.*, *15*(1), 19–36.
Wanner, O., and W. Gujer (1986), A multispecies biofilm model, *Biotechnol. Bioeng.*, *28*(3), 314–328.
Zarnetske, J. P., R. Haggerty, S. M. Wondzell, and M. A. Baker (2011), Labile dissolved organic carbon supply limits hyporheic denitrification, *J. Geophys. Res.*, *116*, G04036, doi:10.1029/2011JG001730.
Zarnetske, J. P., R. Haggerty, S. M. Wondzell, V. A. Bokil, and R. González-Pinzón (2012), Coupled transport and reaction kinetics control the nitrate source-sink function of hyporheic zones, *Water Resour. Res.*, *48*, W11508, doi:10.1029/2012WR011894.